energy&fuels

Article

pubs.acs.org/EF

Observations and Assessment of Fly Ashes from High-Sulfur Bituminous Coals and Blends of High-Sulfur Bituminous and Subbituminous Coals: Environmental Processes Recorded at the Macro- and Nanometer Scale

Jennifer Wilcox,[†] Beibei Wang,[†] Erik Rupp,[†] Ross Taggart,[‡] Heileen Hsu-Kim,[‡] Marcos L. S. Oliveira,[§] César M. N. L. Cutruneo,[§] Silvio Taffarel,[§] Luis F. O. Silva,[§] Shelley D. Hopps,[∥] Gerald A. Thomas,[∥] and James C. Hower*[,∥]

[†]Department of Energy Resources Engineering, Stanford University, Stanford, California 94305-2220, United States

[‡]Department of Civil and Environmental Engineering, Duke University, Durham, North Carolina 27708-0287, United States

[§]Laboratory of Environmental Researches and Nanotechnology Development, Mestrado em Avaliação de Impactos Ambientais em Mineração, Centro Universitário La Salle, Victor Barreto, 2288 Centro 92010-000 Canoas, Rio Grande do Sul, Brazil

[∥]Center for Applied Energy Research, University of Kentucky, 2540 Research Park Drive, Lexington, Kentucky 40511, United States

ABSTRACT: Fly ash was investigated with a variety of chemical, mineralogical, petrographic, and microbeam techniques from three coal-fired units at two Kentucky power plants. Two units burn high-sulfur Illinois Basin high volatile bituminous (hvb) coal, and the third unit burns a ~70:30 blend of high-sulfur Illinois Basin hvb coal and low-sulfur, relatively high-CaO Powder River Basin subbituminous coal. With high-S, high-Fe coals in all of the blends, spinel (magnetite) is an important constituent in the fly ashes. Overall, the fly ashes are dominated by glass. Portlandite was noted in the high-Ca-coal-derived ash. Concentrations of Ba and Sr are highest in the latter fly ash, a function of the Powder River Basin coal source for a portion of the blend. Rare earth elements do not have a high concentration in any of the fly ashes and do not show any significant partitioning between the electrostatic precipitator (ESP) or baghouse rows in the individual generating units. In contrast to previously studied fly ashes from plants burning hvb coals and to other fly ash specimens in this study, the fly ash from the unit burning the Illinois Basin/Powder River Basin coal blend did not have nanoscale carbon on the surface of the spherical inorganic fly ash particles. The absence of carbon may be a function of the nature of the feed coal, with 30% derived from the non-caking sub-bituminous component in the coal blend, although some contribution of carbon derived from caking hvb coal would be expected. The fly ash carbon content is very low, suggesting that the amount of carbon rather than or along with the rank of the coal may be a determining factor in the absence of nanoscale carbon deposition on the surface of the fly ash particles.

1. INTRODUCTION

Pollution of air, water, soils, and sediments with trace hazardous elements is a worldwide problem stemming from many anthropogenic activities, such as fuel mining/processing (e.g., beneficiation) and burning fossil fuels. High concentrations of hazardous elements can also stem from gaseous emissions and solid byproducts from coal-fired power plants.[1−4]

The partitioning and overall capture of trace elements, some of them considered to be hazardous, in coal combustion have been of interest since the passage of the 1990 Clean Air Act amendments, in which a number of elements of environmental concern were named. Foremost among those elements was mercury, regulated in the U.S. through the United States Environmental Protection Agency's (U.S. EPA) Mercury and Air Toxics Standards[5] and Cross-State Air Pollution Rule.[6] A June 29, 2015 U.S. Supreme Court Ruling, however, while not vacating the rules, does require the U.S. EPA to use a stricter cost versus benefit assessment in formulating regulations.[7]

With the exception of Hg,[1] which will not be dealt with in this work, the capture of volatile trace elements by coal-combustion fly ash is generally a function of the flue-gas temperature at the point of capture and the surface area of the fly ash. The flue gas temperature decreases and the fly ash specific surface area increases (concurrent with a decrease in the particle size) toward the back rows of the electrostatic precipitator (ESP) or baghouse arrays, often resulting in an increase in the concentration of the volatile trace elements in fly ash toward the back-row ESP hoppers.[8−28]

Nanoparticles (NPs, e.g., nanominerals or nano-amorphous compounds) measure between roughly 1 nm and several tens of nanometers in all three dimensions.[29] In the natural and/or anthropogenic environmental settings, in many cases, ultrafine and nanominerals have properties that vary from those of the bulk phase.[30−32] These changed complex properties, which may include redox potential and/or sorption capacity, could disturb the availability and biotoxicity of the pollutant within its environment.[29] One of the main explanations that coal fly ash NPs are so reactive is that, as the size of a particle reduces, the ratio of its surface area to volume increases dramatically, thereby increasing the amount of surface available for reactions.[3,33,34]

Received: September 8, 2015
Revised: October 22, 2015
Published: October 26, 2015

DOI: 10.1021/acs.energyfuels.5b02033
Energy Fuels 2015, 29, 7168−7177

Table 1. Fly Ash Petrology (Constituents Listed in Volume Percent)

plant	E	E	E	E	E	E	E	E
unit	2	2	2	2	2	2	2	2
type	ESP	ESP	ESP	ESP	ESP	ESP	ESP	ESP
row	1	1	2	2	3	3	4	4
bin	A4	A6	A12	A14	A20	A22	A28	A30
sample	93604	93605	93606	93607	93608	93609	93610	93611
glass	80.4	82.8	90.8	70.0	87.2	90.8	94.4	91.2
mullite	0.0	0.0	0.0	0.0	0.0	0.0	0.0	0.0
spinel	18.8	15.2	8.8	23.2	10.4	8.4	4.4	6.4
quartz	0.4	1.2	0.4	5.6	0.4	0.8	0.0	1.2
sulfide	0.0	0.0	0.0	0.0	0.0	0.0	0.0	0.0
sulfate	0.0	0.0	0.0	0.0	0.0	0.0	0.0	0.0
crystalline silicate	0.0	0.0	0.0	0.0	0.0	0.0	0.0	0.0
lime	0.0	0.0	0.0	0.0	0.0	0.0	0.0	0.0
rock fragment	0.4	0.0	0.0	0.0	0.0	0.0	0.0	0.0
total inorganics	100.0	99.2	100.0	98.8	98.0	100.0	98.8	98.8
isotropic coke	0.0	0.4	0.0	0.8	0.4	0.0	0.4	0.4
anisotropic coke	0.0	0.4	0.0	0.4	0.8	0.0	0.8	0.4
inertinite	0.0	0.0	0.0	0.0	0.8	0.0	0.0	0.0
total carbon	0.0	0.8	0.0	1.2	2.0	0.0	1.2	0.8

plant	R	R	R	R	R	R
unit	1	1	1	1	1	1
type	ESP	ESP	ESP	ESP	ESP	ESP
row	1	1	2	2	3	3
bin	A515	A520	A516	A521	A517	A522
sample	93628	93629	93630	93631	93632	93633
glass	88.4	87.2	83.2	82.8	83.6	89.2
mullite	0.0	0.0	0.0	0.0	0.4	0.0
spinel	11.2	11.2	14.8	16.4	14.4	6.8
quartz	0.4	0.0	0.0	0.0	0.8	0.4
sulfide	0.0	0.8	0.0	0.4	0.0	0.0
sulfate	0.0	0.0	0.0	0.0	0.0	0.0
crystalline silicate	0.0	0.0	0.0	0.0	0.0	0.0
lime	0.0	0.0	0.0	0.0	0.0	0.0
rock fragment	0.0	0.0	0.0	0.0	0.0	0.0
total inorganics	100.0	99.2	98.0	99.6	99.2	96.4
isotropic coke	t	0.4	0.4	0.4	0.8	3.2
anisotropic coke	0.0	0.0	0.4	0.0	0.0	0.0
inertinite	t	0.4	1.2	0.0	0.0	0.4
total carbon	0.0	0.8	2.0	0.4	0.8	3.6

plant	R	R	R	R	R	R	R	R	R	R	R	R
unit	2	2	2	2	2	2	2	2	2	2	2	2
type	FF	FF	FF	FF	FF	FF	FF	FF	FF	FF	FF	FF
row	1	1	1	1	2	2	2	2	3	3	3	3
bin	2A11-2	2A11-1	2A21-2	2A21-1	2A12-2	2A12-1	2A22-2	2A22-1	2A13-2	2A13-1	2A23-2	2A23-1
sample	93636	93637	93638	93639	93640	93641	93642	93643	93644	93645	93646	93647
glass	87.6	88.8	82.4	94.8	92.4	92.8	93.2	87.6	89.6	89.6	84.0	89.2
mullite	0.0	0.0	0.0	0.0	0.4	0.0	0.0	0.0	0.4	0.0	0.0	0.0
spinel	10.4	10.0	16.0	4.0	6.0	5.6	5.6	8.8	8.0	8.8	14.4	8.0
quartz	2.0	0.8	0.8	0.4	0.4	0.8	0.4	0.4	2.0	0.0	0.4	1.2
sulfide	0.0	0.0	0.0	0.0	0.0	0.0	0.0	0.0	0.0	0.0	0.0	0.0
sulfate	0.0	0.0	0.0	0.0	0.0	0.0	0.0	0.0	0.0	0.0	0.0	0.0
crystalline silicate	0.0	0.0	0.0	0.0	0.0	0.0	0.0	0.0	0.0	0.0	0.0	0.0
lime	0.0	0.0	0.0	0.0	0.0	0.0	0.0	0.0	0.0	0.0	0.0	0.0
rock fragment	0.0	0.0	0.0	0.0	0.0	0.0	0.0	0.0	0.0	0.0	0.0	0.0
total inorganics	100.0	99.6	99.2	99.2	99.2	99.2	99.2	96.8	100.0	98.4	98.8	98.4
isotropic coke	0.0	0.0	0.8	0.8	0.8	0.4	0.0	2.8	0.0	0.4	0.8	1.6
anisotropic coke	0.0	0.0	0.0	0.0	0.0	0.0	0.0	0.4	0.0	0.0	0.0	0.0
inertinite	0.0	0.4	0.0	0.0	0.0	0.0	0.8	0.0	0.0	1.2	0.4	0.0
total carbon	0.0	0.4	0.8	0.8	0.8	0.4	0.8	3.2	0.0	1.6	1.2	1.6

DOI: 10.1021/acs.energyfuels.5b02033
Energy Fuels 2015, 29, 7168−7177

In this study, we are examining the petrology, mineralogy, and chemistry of fly ash from three units at two high-S-coal-fired Kentucky power plants. The units have either been retrofitted (plant E/unit 2) or built specifically (both units at plant R) for the removal of SO_2 from the flue gas stream in compliance with the U.S. EPA's evolving regulations regarding coal-fired power plant emissions. The design of the ash-collection systems combined with the variety of feed coals, with different high-S sources between plants E and R and the blending of subbituminous Powder River Basin coal with the high-S coal at one of the plant R units, provides a simple layout in which to examine the variation in the basic parameters noted above.

2. MATERIALS AND METHODS

Samples of fly ash were collected from three units at two Kentucky power plants in December 2011 and January 2012. The collection, conducted by the University of Kentucky Center for Applied Energy Research (CAER), was part of a pent-annual survey of coal-combustion product production and utilization. The survey was supplemented by a collection of coal and coal-combustion products at Kentucky power plants. In its present incarnation, the survey and collection have been conducted since 1992.[15,16,18,21,35,36]

The power plants are designated by letters, as used in our previous studies of Kentucky power plants. Plant E/unit 2 and Plant R/unit 1 burn high volatile bituminous (hvb), high-S Illinois Basin coal, and Plant R/unit 2 burns a 70:30 blend of hvb, high-S Illinois Basin and sub-bituminous, low-S Powder River Basin (PRB) coal. Unit 2 at plant E and unit 1 at plant R both employ ESPs to separate the fly ash from the flue gas stream. Plant R unit 2 uses an array of baghouses (fabric filters) to remove the fly ash from the flue gas stream. In the CAER collections, sampling of fly ash is from individual hoppers. As best as possible, all rows of the ash collection system are represented. Further, in cases where it was not practical to sample all of the hoppers, sampling followed straight paths within the ESP array. For example, in plant E, samples 93604, 93606, 93608, and 93610 are in a straight path from the hotter (93604) to cooler (93610) end of the ESP array (likewise, the odd-numbered samples also represent a straight path).

Moisture, ash, and carbon analyses (the latter from the ultimate analysis) were conducted at the CAER. Major oxide and minor element concentrations were quantified by X-ray fluorescence at the CAER following procedures outlined by Hower and Bland.[37] The rare earth elements + yttrium (REY) were extracted from the fly ash samples by heated digestion with a 1:1 HF/HNO_3 acid mixture followed by analysis by inductively couple plasma mass spectrometry (Agilent Technologies 7700) at Duke University. The efficiency of this analysis method was tested on fly ash standard reference material (NIST SRM 1633c) that was digested and analyzed in parallel to the samples for this study. Average recoveries of individual REY elements were 89.3−103.4% of the reference concentrations (for Dy, Eu, La, Lu, Sc, and Tb) and information mass concentrations (for Ce, Nd, Sm, and Yb) for SRM 1633c.

Fly ash petrology was performed on epoxy-bound pellets prepared to a final 0.05 μm alumina polish using 50×, reflected-light, oil-immersion optics on Leitz Orthoplan microscopes at the CAER following procedures described by Hower.[38]

Mineralogy was performed at the University of Santiago de Compostela, Galicia, Spain, on a Philips-type powder diffractometer fitted with Philips "PW1710" control unit, Vertical Philips "PW1820/00" goniometer, and FR590 Enraf Nonius generator. The instrument was equipped with a graphite diffracted-beam monochromator and copper radiation source [$\lambda(K\alpha_1)$ = 1.5406 Å], operating at 40 kV and 30 mA. The X-ray powder diffraction pattern (XRPD) was collected by measuring the scintillation response to Cu Kα radiation versus the 2θ value over a 2θ range of 2−65°, with a step size of 0.02° and counting time of 3 s per step.

Microbeam studies of the fly ashes were conducted at the Centro Universitário La Salle, Canoas, Rio Grande do Sul, Brazil, following procedures established by Silva et al.[34] after methods by Giannuzzi et al.[39] The equipment consisted of a dual beam focused ion beam (FIB) of FEI DualBeam Helios 600 Nanolab equipped with (1) a high-resolution field emission gun (FEG) for scanning electron microscopy (SEM), (2) multiple electron detectors for image acquisition, such as through-the-lens detector (TLD), an Everhart−Thornley detector (ETD), and a backscattered electron detector (BSED) for compositional information, and (3) a high-resolution focused Ga^+ ion beam to precisely select, slice, and image a specific region of the species of interest, with a spatial resolution within the 10 nm range.

Morphology, structure, and composition of the fly ash samples were investigated using Zeiss model ULTRA plus field-emission scanning electron microscopy (FE-SEM), with charge compensation for all applications on conductive as well as non-conductive samples, and 200 keV JEOL-2010F high-resolution transmission electron microscopy (HR-TEM), equipped with an Oxford energy-dispersive X-ray detector and a scanning (STEM) unit. FE-SEM was equipped with an energy-dispersive X-ray spectrometer (EDS), and the mineral identifications were made on the basis of morphology and grain composition using both secondary electron and backscattered electron modes. EDS spectra were recorded in TEM image mode and then quantified using ES Vision software that uses the thin foil method to convert X-ray counts of each element into atomic or weight percentages. Electron diffraction patterns of the crystalline phases were recorded in selected area electron diffraction (SAED) or microbeam diffraction (MBD) mode, and the d spacings were compared to the International Centre for Diffraction Data (ICDD)[40] inorganic compound powder diffraction file (PDF) database to identify the crystalline phases.

HR-TEM was carried out at the Stanford Nanocharacterization Laboratory (SNL; http://web.stanford.edu/group/snl/tecnai.htm). The fly ash sample was deposited onto a carbon support film on a Cu TEM grid. TEM observations were made using a FEI Tecnai TEM TF20 at 200 kV (SNL, undated). Energy-dispersive X-ray spectroscopy (EDX) analysis was carried out using an EDAX Genesis spectrometer.

3. RESULTS AND DISCUSSION

3.1. Petrology. The petrology of the fly ash is presented in Table 1. The plant E/unit 2 fly ash is dominated by varying amounts of glass and spinel (Figure 1A) with lesser amounts of quartz and carbon. Samples 93606 and 93607, from the second ESP row, are a good illustration of the asymmetry of the fly ash flow through the ESPs, with significantly more spinel, quartz,

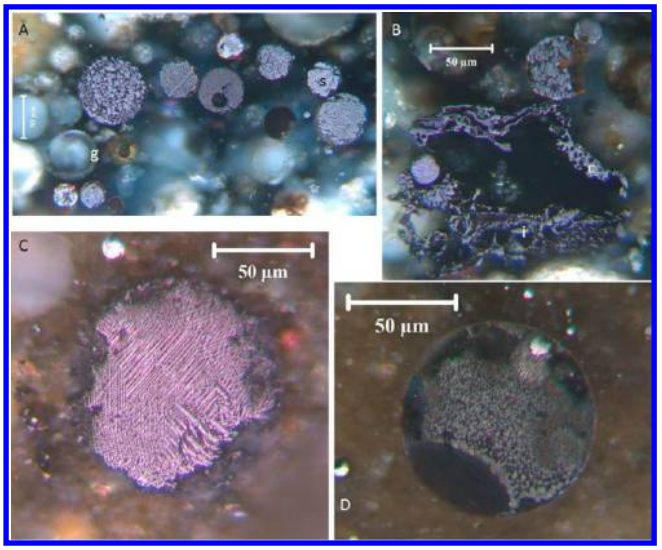

Figure 1. Fly ash petrology: (A) spinel (s) and glass cenospheres (g) (image 93605 02, plant E/unit 2/row 1), (B) inertinite (i) and isotropic coke (c) (image 93607 02, plant E/unit 2/row 2), (C) spinel (image 93628 01, plant R/unit 1/row 1), and (D) spinel in glass (image 93647 02, plant R/unit 2/row 3).

DOI: 10.1021/acs.energyfuels.5b02033
Energy Fuels 2015, 29, 7168−7177

Table 2. Ash, Moisture, and Carbon (%, As-Determined Basis), Major Oxides (%, Ash Basis), and Minor Elements (ppm, Ash Basis)

plant	unit	row	bin	number	ash	moisture	C	SiO_2	Al_2O_3	Fe_2O_3	CaO	MgO	Na_2O	K_2O	P_2O_5	TiO_2	SO_3
E	2	1	A4	93604	98.99	0.06	<0.1	48.25	20.16	23.02	4.06	1.22	0.32	1.90	0.08	0.96	0.31
E	2	1	A6	93605	99.21	0.04	<0.1	47.67	19.96	23.36	4.21	1.22	0.30	1.83	0.08	0.94	0.22
E	2	2	A12	93606	99.11	0.04	0.05	49.73	22.73	17.72	3.65	1.31	0.37	2.28	0.13	1.06	0.46
E	2	2	A14	93607	99.24	0.03	0.04	46.97	19.95	23.93	4.27	1.20	0.31	1.84	0.08	0.95	0.48
E	2	3	A20	93608	98.78	0.07	0.25	49.98	23.72	15.59	3.72	1.41	0.41	2.43	0.20	1.09	0.89
E	2	3	A22	93609	98.97	0.04	0.29	49.83	22.50	18.61	3.70	1.30	0.36	2.21	0.11	1.05	0.43
E	2	4	A28	93610	98.72	0.12	<0.1	46.86	24.54	13.83	4.47	1.49	0.46	2.54	0.39	1.14	2.63
E	2	4	A30	93611	98.83	0.05	0.24	50.88	23.89	15.91	3.71	1.39	0.40	2.42	0.18	1.10	0.79

plant	unit	row	bin	number	V	Cr	Mn	Co	Ni	Cu	Zn	As	Rb	Sr	Zr	Mo	Cd	Sb	Ba	Pb	Ga	Ag	Tl	Th	U
E	2	1	A4	93604	297	140	283	69	86	64	87	82	23	284	16	<1	1	7	640	33		0.5	2.5	18.3	13.6
E	2	1	A6	93605	284	137	289	70	86	61	78	73	59	244	16	<1	1	8	636	30		0.4	1.3	14.4	9.7
E	2	2	A12	93606	334	145	246	56	90	109	164	134	29	451	13	49	1	5	627	65		0.9	6.9	20.7	14.8
E	2	2	A14	93607	304	140	293	72	89	67	84	79	39	255	16	<1	1	8	644	31	15.2		1.6	15.0	10.8
E	2	3	A20	93608	382	150	247	51	96	136	227	201	36	516	12	78	1	5	692	97		1.4	9.9	17.4	13.9
E	2	3	A22	93609	333	144	250	58	90	104	146	119	38	422	13	36	1	5	623	57	32.5		5.0	16.0	11.6
E	2	4	A28	93610	544	166	264	49	114	183	378	359	9	559	11	141	1	3	905	161		1.9	26.7	25.2	25.9
E	2	4	A30	93611	374	151	247	52	96	132	210	182	31	511	12	77	1	4	678	89		1.1	8.9	18.0	13.8

plant	unit	row	bin	number	Sc	Y	La	Ce	Pr	Nd	Sm	LREE	Eu	Gd	Tb	Dy	Ho	Er	Tm	Yb	Lu	HREE	Y + REE	LREE/HREE
E	2	1	A4	93604	28.5	61.4	61.0	127.3	14.3	57.0	11.7	271.3	2.5	11.6	1.7	10.0	2.0	5.7	0.8	5.2	0.8	40.4	373.1	6.72
E	2	1	A6	93605	23.1	47.8	49.2	101.6	11.3	45.2	9.3	216.6	2.0	9.3	1.3	7.7	1.6	4.4	0.6	4.0	0.6	31.5	295.9	6.87
E	2	2	A12	93606	34.0	67.6	65.4	136.3	15.3	61.1	12.6	290.7	2.7	12.8	1.9	10.9	2.3	6.4	0.9	5.8	0.9	44.6	402.9	6.52
E	2	2	A14	93607	22.1	46.9	47.6	104.7	11.6	43.4	9.2	216.4	2.0	9.2	1.4	8.2	1.7	4.8	0.7	4.3	0.6	32.8	296.1	6.60
E	2	3	A20	93608	29.3	57.1	55.3	113.8	12.8	50.9	10.6	243.4	2.3	10.7	1.6	9.2	1.9	5.4	0.8	4.9	0.7	37.4	337.9	6.51
E	2	3	A22	93609	28.7	54.3	56.2	116.0	13.0	49.1	10.2	244.5	2.3	10.4	1.6	9.2	1.9	5.5	0.8	4.9	0.7	37.3	336.1	6.55
E	2	4	A28	93610	40.1	84.2	78.1	161.1	18.2	73.2	15.3	345.9	3.3	15.7	2.3	13.5	2.8	7.9	1.1	7.0	1.1	54.8	484.9	6.31
E	2	4	A30	93611	30.6	59.6	57.1	118.7	13.2	52.9	11.0	252.7	2.3	11.1	1.6	9.5	2.0	5.6	0.8	5.0	0.8	38.7	351.0	6.53

plant	unit	row	bin	number	ash	moisture	C	SiO_2	Al_2O_3	Fe_2O	CaO	MgO	Na_2O	K_2O	P_2O_5	TiO_2	SO_3
R	1	1	AS15	93628	99.23	0.13	<0.1	49.46	21.14	19.53	5.07	1.00	0.49	2.24	0.20	1.03	1.48
R	1	1	AS20	93629	99.23	0.15	<0.1	49.72	21.95	18.77	4.02	0.97	0.46	2.33	0.18	1.06	1.65
R	1	2	AS16	93630	98.69	0.42	<0.1	49.25	21.89	18.42	4.20	0.99	0.40	2.31	0.18	1.05	1.61
R	1	2	AS21	93631	99.02	0.14	0.12	48.20	20.35	18.44	6.41	0.98	0.64	2.21	0.19	1.01	2.39
R	1	3	AS17	93632	99.01	0.15	0.09	50.03	21.80	18.13	4.67	0.96	0.45	2.22	0.16	1.04	1.95
R	1	3	AS22	93633	98.87	0.19	<0.1	49.54	21.78	17.32	5.22	0.98	0.49	2.28	0.20	1.04	3.10

plant	unit	row	bin	number	V	Cr	Mn	Co	Ni	Cu	Zn	As	Rb	Sr	Zr	Mo	Cd	Sb	Ba	Pb	Ga	Ag	Tl	Th	U
R	1	1	AS15	93628	370	159	269	60	108	62	265	111	50	322	15	33	1	7	689	50	40.1	0.6	7.5	18.2	18.0
R	1	1	AS20	93629	365	160	240	59	110	71	283	118	48	318	14	50	1	6	623	56	41.3	0.6	7.8	17.1	16.3
R	1	2	AS16	93630	337	158	236	58	109	63	305	124	45	358	14	42	1	6	642	59	43.3	0.6	8.5	17.7	15.7
R	1	2	AS21	93631	441	162	296	57	107	60	302	115	81	190	15	44	1	7	744	53	39.7	1.1	9.3	16.2	20.8
R	1	3	AS17	93632	385	157	253	57	104	63	297	118	78	276	15	41	1	6	705	57	39.8	0.6	9.0	17.7	18.1
R	1	3	AS22	93633	404	160	248	55	107	63	322	132	73	278	14	58	1	6	723	63	45.6	0.6	11.4	16.9	18.5

plant	unit	row	bin	number	Sc	Y	La	Ce	Pr	Nd	Sm	LREE	Eu	Gd	Tb	Dy	Ho	Er	Tm	Yb	Lu	HREE	Y + REE	LREE/HREE
R	1	1	AS15	93628	30.3	61.5	60.2	122.9	13.8	52.6	11.2	260.7	2.6	11.1	1.8	10.5	2.1	6.1	0.9	5.7	0.8	41.6	363.8	6.26
R	1	1	AS20	93629	28.3	59.0	55.7	115.6	13.0	49.6	10.5	244.5	2.4	10.6	1.7	9.8	2.0	5.8	0.8	5.2	0.8	39.1	342.6	6.25

DOI: 10.1021/acs.energyfuels.5b02033
Energy Fuels 2015, 29, 7168−7177

Table 2. continued

plant	unit	row	bin	number	Sc	Y	La	Ce	Pr	Nd	Sm	LREE	Eu	Gd	Tb	Dy	Ho	Er	Tm	Yb	Lu	HREE	Y + REE	LREE/HREE
R	1	2	A516	93630	29.6	60.6	58.1	119.4	13.5	52.4	10.9	254.3	2.4	11.1	1.8	10.2	2.1	6.0	0.9	5.4	0.8	40.8	355.8	6.23
R	1	2	A521	93631	29.6	56.0	52.7	108.0	12.0	45.9	9.6	228.1	2.2	9.5	1.5	9.1	1.9	5.4	0.8	5.0	0.8	36.3	320.4	6.29
R	1	3	A517	93632	28.6	60.2	59.7	121.2	13.6	51.4	10.7	256.5	2.4	10.6	1.7	10.2	2.0	6.1	0.9	5.4	0.8	40.1	356.8	6.39
R	1	3	A522	93633	29.4	58.1	55.9	114.8	12.9	49.7	10.5	243.7	2.3	10.5	1.6	9.6	2.0	5.7	0.8	5.2	0.8	38.5	340.3	6.33

plant	unit	row	bin	number	ash	moisture	C	SiO_2	Al_2O_3	Fe_2O3	CaO	MgO	Na_2O	K_2O	P_2O	TiO_2	SO_3
R	2	1	2A11-2	93636	98.07	0.12	0.31	46.04	18.74	15.76	11.55	1.59	0.80	1.80	0.29	0.96	2.52
R	2	1	2A11-1	93637	98.90	0.13	<0.1	46.22	19.20	15.47	10.86	1.64	0.84	1.89	0.26	1.01	2.59
R	2	1	2A21-2	93638	98.96	0.16	<0.1	46.14	19.44	14.99	10.49	1.71	0.81	1.90	0.30	1.01	2.68
R	2	1	2A21-1	93639	97.35	0.23	0.93	44.84	19.15	14.90	11.83	1.64	0.84	1.85	0.31	1.00	3.19
R	2	2	2A12-2	93640	98.96	0.14	<0.1	46.85	19.08	15.94	10.54	1.66	0.75	1.85	0.33	0.97	2.34
R	2	2	2A12-1	93641	98.51	0.17	0.06	45.70	19.36	15.14	10.60	1.63	0.83	1.90	0.28	1.01	2.87
R	2	2	2A22-2	93642	98.64	0.17	<0.1	45.34	19.43	14.75	11.04	1.64	0.84	1.88	0.31	1.01	3.32
R	2	2	2A22-1	93643	98.67	0.16	0.04	46.01	19.66	15.04	10.52	1.61	0.82	1.91	0.30	1.01	3.33
R	2	3	2A13-2	93644	98.75	0.20	<0.1	43.98	19.19	15.24	11.62	1.68	0.74	1.73	0.41	0.98	4.36
R	2	3	2A13-1	93645	98.67	0.17	<0.1	44.27	19.70	14.81	11.24	1.67	0.81	1.86	0.34	1.01	3.98
R	2	3	2A23-2	93646	98.11	0.51	<0.1	43.19	19.71	14.28	11.12	1.73	0.87	1.84	0.34	1.01	4.66
R	2	3	2A23-1	93647	98.30	0.42	<0.1	43.40	19.60	14.39	10.76	1.72	0.87	1.83	0.35	1.00	4.57

plant	unit	row	bin	number	V	Cr	Mn	Co	Ni	Cu	Zn	As	Rb	Sr	Zr	Mo	Cd	Sb	Ba	Pb	Ga	Ag	Tl	Th	U
R	2	1	2A11-2	93636	386	135	264	47	89	57	274	74	129	509	15	15	1	8	1333	40	30.6	0.6	6.3	16.2	20.1
R	2	1	2A11-1	93637	414	138	284	47	92	60	303	75	89	577	14	44	1	7	1340	42	32.8	0.6	6.7	16.0	20.2
R	2	1	2A21-2	93638	413	137	282	46	94	61	333	74	94	640	13	47	1	7	1426	43	32.7	0.6	6.7	16.0	19.5
R	2	1	2A21-1	93639	429	139	284	45	93	62	326	76	66	665	13	63	1	6	1544	42	32.8	0.6	8.3	16.1	20.7
R	2	2	2A12-2	93640	404	134	307	48	91	56	287	72	94	602	14	33	1	7	1503	40	30.4	0.6	7.0	16.2	20.7
R	2	2	2A12-1	93641	429	139	282	47	94	63	327	78	72	632	13	58	1	6	1436	44	35.0	0.6	7.7	16.0	20.3
R	2	2	2A22-2	93642	456	142	285	45	95	64	343	78	68	655	13	65	1	6	1547	44	34.8	0.6	8.0	15.4	20.7
R	2	2	2A22-1	93643	449	142	283	46	103	63	335	82	66	633	13	67	1	6	1433	45	38.1	0.7	8.6	16.9	22.0
R	2	3	2A13-2	93644	518	143	319	46	95	65	363	85	98	631	14	48	1	7	1890	45	39.2	1.1	12.4	15.8	24.5
R	2	3	2A13-1	93645	508	145	295	46	97	67	372	87	67	676	13	71	1	6	1740	47	44.0	0.7	12.0	17.3	25.2
R	2	3	2A23-2	93646	621	150	286	44	100	69	412	98	105	683	13	25	1	6	1710	53	43.7	0.7	12.0	16.2	23.8
R	2	3	2A23-1	93647	625	150	287	45	101	68	404	98	163	590	15	15	1	8	1628	54	44.2	0.7	12.2	15.9	23.9

plant	unit	row	bin	number	Sc	Y	La	Ce	Pr	Nd	Sm	LREE	Eu	Gd	Tb	Dy	Ho	Er	Tm	Yb	Lu	HREE	Y + REE	LREE/HREE
R	2	1	2A11-2	93636	26.2	46.7	50.0	101.0	11.1	41.4	8.4	211.9	2.0	8.4	1.3	8.0	1.7	4.9	0.7	4.5	0.7	32.3	290.9	6.56
R	2	1	2A11-1	93637	27.0	46.2	48.2	99.6	10.8	40.6	8.2	207.4	2.0	8.2	1.3	8.1	1.7	5.0	0.7	4.6	0.7	32.3	285.9	6.43
R	2	1	2A21-2	93638	25.9	45.9	49.3	98.9	10.9	40.8	8.2	208.1	2.0	8.3	1.3	8.0	1.6	4.8	0.7	4.5	0.7	32.0	285.9	6.51
R	2	1	2A21-1	93639	24.9	46.0	46.7	99.0	10.9	40.7	8.2	205.6	2.1	8.3	1.3	8.0	1.7	4.9	0.7	4.6	0.7	32.1	283.6	6.41
R	2	2	2A12-2	93640	26.4	46.4	50.5	101.8	11.2	42.0	8.4	214.0	2.1	8.3	1.3	7.9	1.6	4.9	0.7	4.5	0.7	31.8	292.1	6.73
R	2	2	2A12-1	93641	26.7	46.9	49.4	101.0	10.9	41.1	8.3	210.7	2.0	8.3	1.3	8.1	1.7	4.9	0.7	4.6	0.7	32.3	289.8	6.53
R	2	2	2A22-2	93642	27.0	44.9	47.0	95.6	10.5	39.4	7.9	200.3	2.0	7.9	1.2	7.6	1.6	4.7	0.7	4.4	0.7	30.7	275.9	6.53
R	2	2	2A22-1	93643	27.3	48.9	52.9	106.8	11.8	43.9	8.8	224.2	2.2	8.8	1.4	8.5	1.8	5.2	0.8	4.8	0.7	34.1	307.2	6.58
R	2	3	2A13-2	93644	27.2	46.1	50.6	102.5	11.2	42.0	8.5	214.7	2.1	8.5	1.3	7.9	1.6	4.8	0.7	4.4	0.7	32.0	292.8	6.70
R	2	3	2A13-1	93645	28.2	51.2	54.8	110.4	12.1	45.3	9.0	231.7	2.3	9.0	1.4	8.7	1.8	5.2	0.8	4.9	0.7	34.8	317.7	6.65
R	2	3	2A23-2	93646	27.8	47.8	50.7	102.6	11.3	41.5	8.4	214.5	2.2	8.4	1.3	8.3	1.7	5.0	0.8	4.7	0.7	33.0	295.2	6.50
R	2	3	2A23-1	93647	27.3	46.9	50.0	100.5	11.0	41.2	8.3	211.0	2.1	8.3	1.3	8.1	1.7	4.9	0.7	4.6	0.7	32.4	290.3	6.52

DOI: 10.1021/acs.energyfuels.5b02033
Energy Fuels 2015, 29, 7168−7177

Table 3. Minerals Detected by X-ray Diffraction (XRD)

plant	unit	row	bin	sample	anhydrite	calcium oxide	hematite	maghemite	magnetite	mullite	portlandite	quartz
E	2	1	A4	93604		×	×	×		×		×
E	2	1	A6	93605		×	×	×		×		×
E	2	2	A12	93606	×	×	×	×		×		×
E	2	2	A14	93607	×	×	×	×		×		×
E	2	3	A20	93608	×	×	×	×		×		×
E	2	3	A22	93609	×	×	×	×		×		×
E	2	4	A58	93610	×	×	×	×		×		×
E	2	4	A30	93611	×	×	×	×		×		×
R	1	1	A515	93628	×	×	×	×	×	×	×	×
R	1	1	A520	93629	×	×	×	×	×	×	×	×
R	1	2	A516	93630	×	×	×	×	×	×		×
R	1	2	A521	93631	×	×	×	×	×	×		×
R	1	3	A517	93632	×	×	×	×	×	×	×	×
R	1	3	A522	93633	×	×	×	×	×	×	×	×
R	2	1	2A11-2	93636	×	×	×	×		×	×	×
R	2	1	2A11-1	93637	×	×	×	×		×	×	×
R	2	1	2A21-2	93638	×	×	×	×		×	×	×
R	2	1	2A21-1	93639	×	×	×	×		×	×	×
R	2	2	2A12-2	93640	×	×	×	×		×	×	×
R	2	2	2A12-1	93641	×	×	×	×		×	×	×
R	2	2	2A22-2	93642	×	×	×	×		×	×	×
R	2	2	2A22-1	93643	×	×	×	×		×	×	×
R	2	3	2A13-2	93644	×	×	×	×		×	×	×
R	2	3	2A13-1	93645	×	×	×	×		×	×	×
R	2	3	2A23-2	93646	×	×	×	×		×	×	×
R	2	3	2A23-1	93647	×	×	×			×	×	×

and carbon (Figure 1B) in sample 93607. Spinels, with varying amounts of associated glass, are also present in the plant R fly ashes (panels C and D of Figure 1).

3.2. Chemistry and Mineralogy. The fly ash chemistry is shown on Table 2. None of the ashes was high in carbon, a positive trend for potential utilization, with only a plant R/unit 2/baghouse row 1 sample approaching 1% C. The amount of Fe, however, generally tied up with the spinel fraction (see section 3.1), might be detrimental to some potential uses of the fly ash as a result of the dark color associated with high-Fe fly ashes. As a general indicator of the capture of volatile species, SO_3 is generally but not consistently highest in the back row of the ash-collection system. The plant E/unit 2 fly ash shows higher concentrations of Zn and As in the ESP rows 3 and 4, in the back, cooler end of the particulate-control system relative to fly ash from rows 1 and 2. This amounts to an approximately 3 times enrichment in the fourth ESP row versus the first ESP row. The plant R units, however, do not show Zn and As enrichment of the same magnitude as in plant E/unit 2. Other investigations of the same unit show similar results, indicating that the lack of a significant partitioning is not unique to this sample suite (unpublished data from 2002 and 2007 collections used in summaries by Hower et al.;[18,21] unpublished data from 2013 collection). The higher CaO of the Powder River Basin portion of the plant R/unit 2 feed coal is reflected in 10.54–11.83% CaO in the fly ash, significantly higher than 4.02–6.41% CaO in the plant R/unit 1 fly ash.

Certain minor elements reflect the differences in the chemistry in the source coals, both between the two solely Illinois Basin sources (plant E/unit 2 and plant R/unit 1) and the latter two coal blends versus the plant R/unit 2 Illinois Basin/PRB blend. For example, considering the Zn distribution between the two Illinois Basin sources, the fly ash at plant R/unit 1 is higher than the plant E/unit 2 fly ash, despite a concentration of 378 ppm in a fourth row ESP hopper at the latter plant. The Sr and Ba concentrations are highest in the plant R/unit 2 fly ash, reflecting the blending of the higher CaO PRB coal with the unit 1 Illinois Basin coal.

Some fly ashes are noted for high concentrations of rare earth elements.[26,41] Within the Pennsylvanian coals of the eastern U.S., Central Appalachian coals, such as the coal run at the plant in the Mardon and Hower study, generally have higher rare earth concentrations than Illinois Basin coals.[42] Therefore, it is not surprising that the rare earth + yttrium (REY) concentrations at these units is low, with only two samples, both from plant E/unit 2, exceeding 400 ppm of REY and only two plant R/unit 2 fly ashes exceeding 300 ppm of REY. There is no partitioning in REY between the ash-collection rows, and unlike the trends noted by Mardon and Hower[26] for another plant, there is no significant change in the light rare earth/heavy rare earth ratio between the rows. Both the low REY concentrations and the lack of partitioning for a sample suite collection in 2007 at plant R/unit 1 confirm the observations made here.[42]

Much of the bulk mineralogy is similar for all hoppers in all three units (Table 3). Magnetite (Fe spinel) is only present in the plant R/unit 1 samples, and portlandite is most abundant in the plant R/unit 2 samples for which the feed coal had 30% CaO (in contrast to the high-S eastern U.S. bituminous coal) feed coal.

FE-SEM was used to discern greater details of the fly ash particles. Sample 93604 from the first row ESP of plant E/unit 2 exhibits a variety of spinel chemistries (Figure 2, particle 1 is a Cr-, As-, V-, and Mn-bearing spinel; Figure 3A is a Ni- and Zn-bearing spinel), carbons (Figure 2, particle 2; Figure 3B), and glassy spheres (Figure 2, multiple particles labeled 3). Plant R/unit 1 shows encapsulation of small (generally) glassy

DOI: 10.1021/acs.energyfuels.5b02033
Energy Fuels 2015, 29, 7168–7177

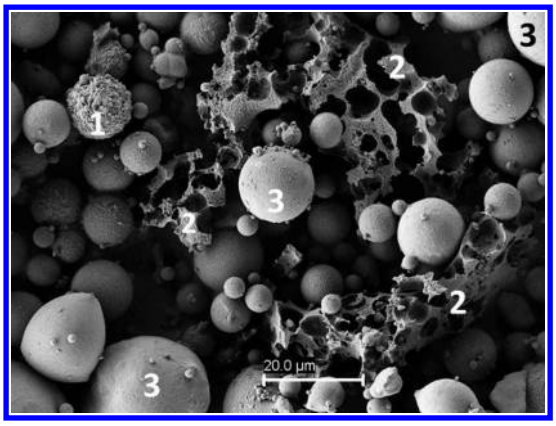

Figure 2. FE-SEM image of sample 93604 (plant E/unit 2/row 1): (1) spinel with Cr, As. V, and Mn, (2) coke, and (3) spheres with Al, Si, Mg, O, K, and Na.

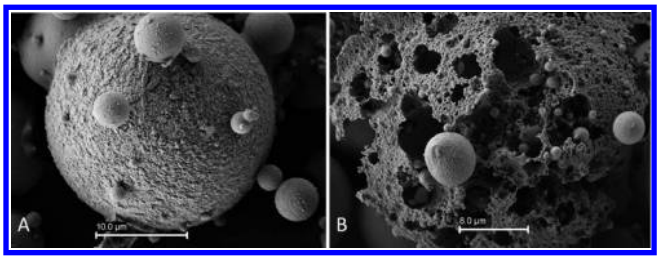

Figure 3. FE-SEM image of sample 93604 (plant E/unit 2/row 1): (A) spinel associated with C, Hg, Ni, and Zn and (B) coke and small spheres, with elemental determination by EDS.

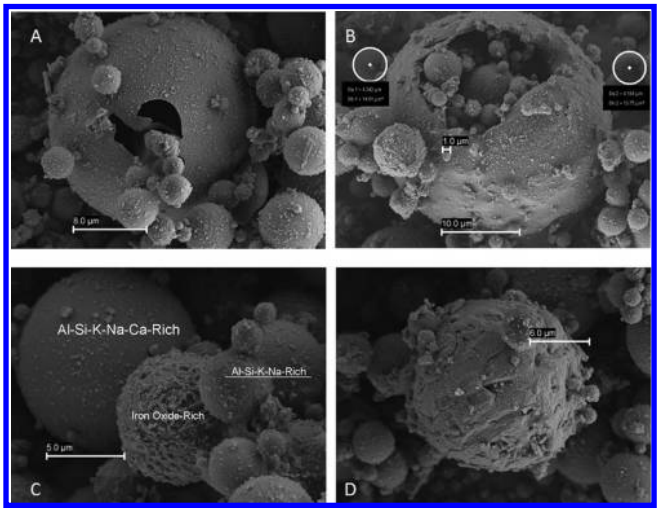

Figure 4. FE-SEM image of sample 93630 (plant R/unit 1/row 2): (A) encapsulation of smaller spheres, (B) encapsulation of smaller spheres, (C) glass (Al–Si–K–Na ± Ca) and spinel spheres, and (D) Fe spinel with Cd, Se, and Co, with elemental determination by EDS.

spheres within cenospheres (panels A and B of Figure 4). The associated glass is composed of Al, Si, K, and Na, with or without Ca (Figure 4C). Iron spinels with Cd, Se, and Co were noted (Figure 4D). Plant R/unit 1/second and third row ESP samples contain gypsum and anhydrite (Figure 5, particle 1) and gypsum with Fe sulfates (Figure 6). A Ca–Al–Si glass with Mn and S was observed (Figure 5, particle 2). Plant R/unit 2/first row baghouse samples have examples of the encapsulation of small spheres within a cenosphere (Figure 7A) and quartz with uncombusted carbon (Figure 7B). TEM/EDX analysis of

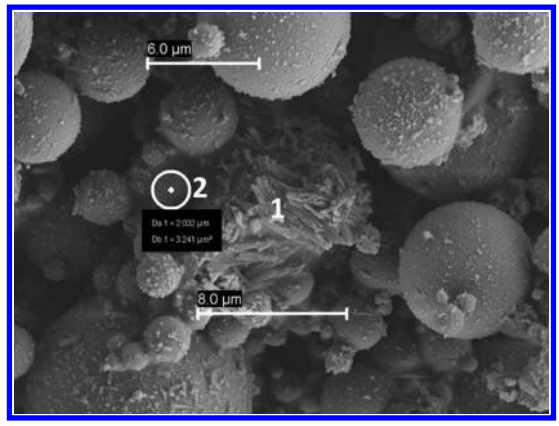

Figure 5. FE-SEM image of sample 93630 (plant R/unit 1/row 2): (1) gypsum and anhydrite and (2) spherical Ca–Si–Al–O particle with Mn and S, with elemental determination by EDS.

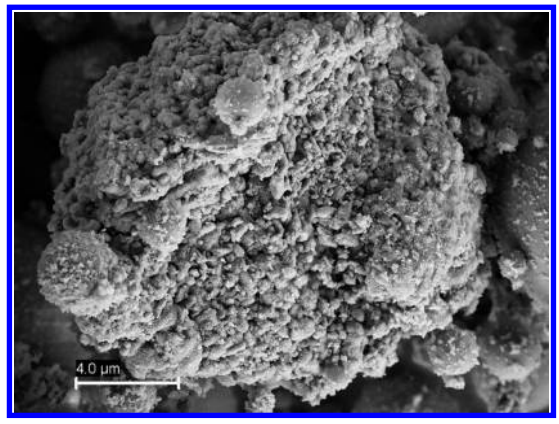

Figure 6. FE-SEM image of sample 93633 (plant R/unit 1/row 3): gypsum mixed with Fe sulfates and Al–Si glass, with elemental determination by EDS.

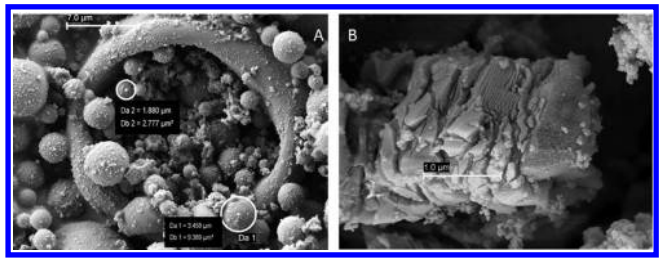

Figure 7. (A) FE-SEM image of sample 93636 (plant R/unit 2/row 1), with encapsulation of smaller spheres, and (B) FE-SEM image of sample 93637 (plant R/unit 2/row 1): quartz with unburned carbon, with elemental determination by EDS.

fly ash confirmed that the plant R/unit 2 fly ashes had greater amounts of Ca associated with particles than the plant E/unit 2 or plant R/unit 1 fly ashes.

HR-TEM of fly ash from plant R/unit 2/baghouse rows 1 and 2 (samples 93637 and 93640, respectively) shows assemblages of fly ash particles with no apparent carbon on the surface of the particles (Figure 8). This contrasts with the observations of Hower et al.[43] and Silva et al.[44] who found abundant fullerene carbons on the surface of fly ashes derived from the combustion of high-volatile A bituminous eastern Kentucky coals. Their fly ashes had significantly more carbon than the samples studied here, <0.01% C in both 93637 and 93640. The paucity of carbon in the latter fly ashes is certainly a factor in the apparent absence of nanoscale

DOI: 10.1021/acs.energyfuels.5b02033
Energy Fuels 2015, 29, 7168–7177

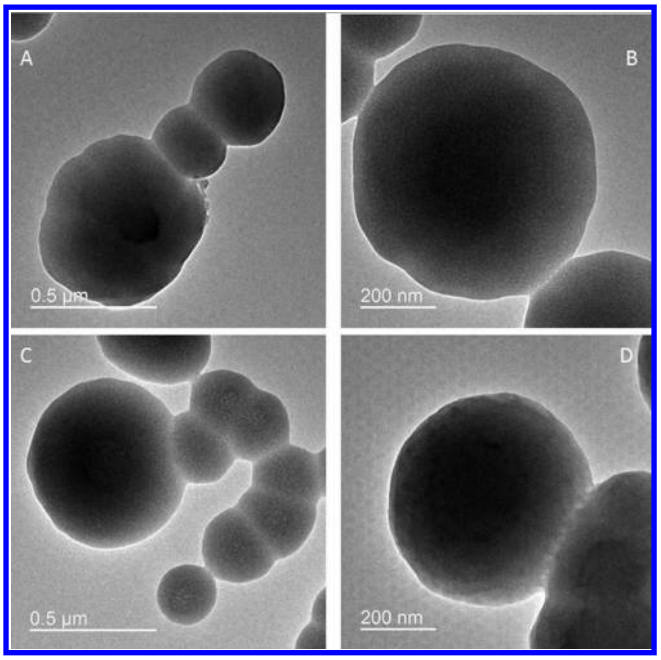

Figure 8. TEM images of particles from (A and B) 93637 and (C and D) 93640 (plant R/unit 2/rows 1 and 2, respectively). Carbon does not appear to be present on the surface of the particles (compare to Figures 9 and 10).

carbon of the surface of the inorganic particles. Another consideration is the fundamental differences between the carbon char derived from the combustion of low-rank coals[33] versus the melted and repolymerized carbon derived from caking coals. However, the subbituminous coal only comprised 30% of the coal blend; the caking bituminous fraction of the blend should be contributing to the overall thermoplastic behavior.

In contrast, particles from sample 93607 (plant E/unit 2/row 2; Figure 9), sample 93630 (plant R/unit 1/row 2; Figure 10), and

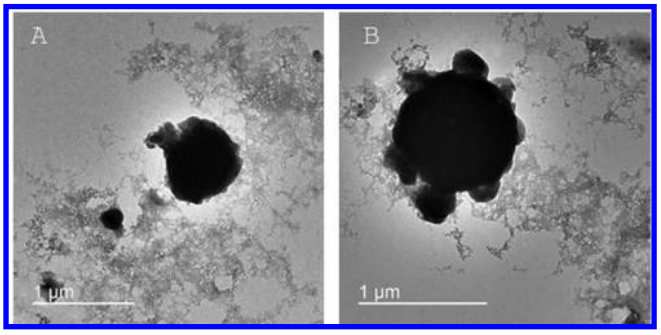

Figure 9. TEM images of particles from 93607 (plant E/unit 2/row 2). Carbon is present on the surfaces of the particles and in the space between the particles.

samples 93643 and 93644 (plant R/unit 2/rows (A and B) 2 and (C and D) 3; Figure 11) all have carbon more-or-less loosely attached to their surfaces. The total fly ash carbon is not an absolute indicator of the presence of the surface carbon; samples 93607 and 93643 have 0.04% C, and samples 93630 and 93644 have <0.01% C. Even the 0.04% C is a very small number compared to the >25% C in the third row fabric filter ash-collection system employed for the samples studied by Silva et al.[44] (data from Mardon et al.[45]).

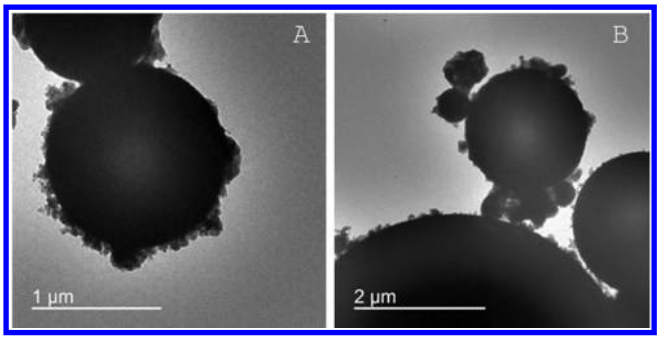

Figure 10. TEM images of particles from 93630 (plant R/unit 1/row 2). Carbon is present on the surfaces of the particles.

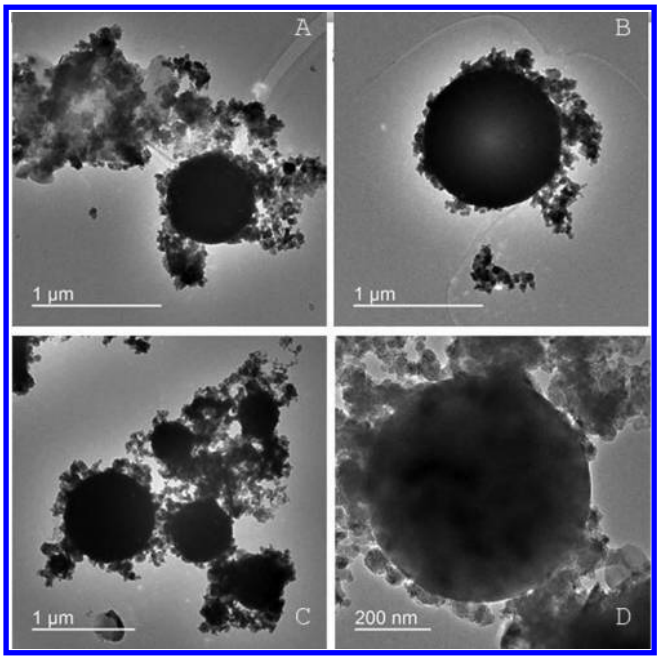

Figure 11. TEM images of particles from (A and B) 93643 and (C and D) 93644 (plant R/unit 2/rows 2 and 3, respectively). Carbon is present on the surfaces of the particles.

4. SUMMARY

Fly ash from three coal-fired units at two Kentucky power plants, with two units burning high-sulfur Illinois Basin hvb coal and the third unit burning a ~70:30 blend of high-sulfur Illinois Basin hvb coal and low-sulfur, relatively high-CaO Powder River Basin subbituminous coal, was investigated with a variety of chemical, mineralogical, petrographic, and microbeam techniques.

The fly ashes are dominated by glass and spinel (magnetite), with some portlandite in the high-Ca-coal-derived ash. Concentrations of Ba and Sr are highest in the latter fly ash, indicating a source from the Powder River Basin coal in the blend. Rare earth elements were not observed in a high concentration in any of the fly ashes and do not show any significant partitioning between the ESP or baghouse rows in the individual generating units.

In contrast to previously studied fly ashes from plants burning hvb coals and to other fly ash specimens in this study, some the fly ash from plant R/unit 2/baghouse rows 1 and 2, the plant burning the Illinois Basin/Powder River Basin coal blend, did not have nanoscale carbon on the surface of the spherical inorganic fly ash particles. The absence of carbon may

DOI: 10.1021/acs.energyfuels.5b02033
Energy Fuels 2015, 29, 7168−7177

be a function of the nature of the feed coal, with 30% of the fuel being from the non-caking subbituminous component in the coal blend. However, some contribution of carbon derived from caking hvb coal would be expected. The overall fly ash carbon content is very low though, implying that the amount of carbon rather than the rank of the coal may be a determining factor in the absence of nanoscale carbon deposition on the surface of the fly ash particles. As noted above, fly ashes from the two units only burning hvb coals as well as plant R/unit 2/baghouse rows 2 and 3 show deposition of nanoscale carbons.

AUTHOR INFORMATION

Corresponding Author

*Telephone: 1-859-257-0261. E-mail: james.hower@uky.edu.

Notes

The authors declare no competing financial interest.

ACKNOWLEDGMENTS

This study was supported in part by the National Science Foundation (CBET-1235661) to the Duke University and University of Kentucky groups. The work performed by the group from Brazil was funded by the National Council of Technological and Scientific Development (CNPq). Luis F. O. Silva and Marcos L. S. Oliveira thank CNPq for scholarships. The authors thank the reviewers and editor, Hongwei Wu, for their constructive comments.

REFERENCES

(1) Hower, J. C.; Senior, C. L.; Suuberg, E. M.; Hurt, R. H.; Wilcox, J. L.; Olson, E. S. Mercury capture by native fly ash carbons in coal fired power plants. *Prog. Energy Combust. Sci.* **2010**, *36*, 510−529.

(2) Kronbauer, M. A.; Izquierdo, M.; Dai, S.; Waanders, F. B.; Wagner, N. J.; Mastalerz, M.; Hower, J. C.; Oliveira, M. L. S.; Taffarel, S. R.; Bizani, D.; Silva, L. F. O. Geochemistry of ultra-fine and nano-compounds in coal gasification ashes: A synoptic view. *Sci. Total Environ.* **2013**, *456*−*457*, 95−103.

(3) Martinello, K.; Oliveira, M. L. S.; Molossi, F. A.; Ramos, C. G.; Teixeira, E. C.; Kautzmann, R. M.; Silva, L. F. O. Direct identification of hazardous elements in ultra-fine and nanominerals from coal fly ash produced during diesel co-firing. *Sci. Total Environ.* **2014**, *470*−*471*, 444−452.

(4) Saikia, B. K.; Ward, C. R.; Oliveira, M. L. S.; Hower, J. C.; Baruah, B. P.; Braga, M.; Silva, L. F. Geochemistry and nano-mineralogy of two medium-sulfur Northeast Indian coals. *Int. J. Coal Geol.* **2014**, *121*, 26−34.

(5) United States Environmental Protection Agency (U.S. EPA). *Mercury and Air Toxics Standards*; U.S. EPA: Washington, D.C., 2012; http://www.epa.gov/mats/ (accessed Jan 20, 2014).

(6) United States Environmental Protection Agency (U.S. EPA). *Cross-State Air Pollution Rule (CSAPR)*; U.S. EPA: Washington, D.C., 2013; http://www.epa.gov/crossstaterule/ (accessed Jan 20, 2014).

(7) Supreme Court of the United States. *Michigan, et al. Petitioners 14-46 v. Environmental Protection Agency et al., Utility Air Regulatory Group, Petitioner 14-17 v. Environmental Protection Agency, et al., National Mining Association, Petitioner 14-49 v. Environmental Protection Agency, et al. on writs of certiorari to the United States Court of Appeals for the District of Columbia Circuit*; Supreme Court of the United States: Washington, D.C., 2015; http://www.supremecourt.gov/opinions/14pdf/14-46_bqmc.pdf.

(8) Meij, R. Trace element behavior in coal fired power plants. *Fuel Process. Technol.* **1994**, *39*, 199−217.

(9) Querol, X.; Fernandez-Turiel, J. L.; Lopez-Soler, A. Trace elements in coal and their behaviour during combustion in a large power station. *Fuel* **1995**, *74*, 331−343.

(10) Bool, L. E., III; Helble, J.J. A laboratory study of the partitioning of trace elements during pulverized coal combustion. *Energy Fuels* **1995**, *9*, 880−887.

(11) Robl, T. L.; Hower, J. C.; Groppo, J. G.; Graham, U. M.; Rathbone, R. F.; Taulbee, D. N.; Medina, S. S. The impact of conversion to low-NO_x burners on ash characteristics. *Proceedings of the International Joint Power Generation Conference*; Minneapolis, MN, Oct 8−12, 1995; Vol. *1*: Environmental Control/Fuels and Combustion Technologies, pp 469−476.

(12) Hower, J. C.; Robl, T. L.; Rathbone, R. F.; Schram, W. H.; Thomas, G.A.. Characterization of pre- and post-NO_x conversion fly ash from the Tennessee Valley Authority's John Sevier Fossil Plant. *Proceedings of the 12th International Symposium on Coal Combustion By-Product (CCB) Management and Use*; Orlando, FL, Jan 26−30, 1997; EPRI TR-107055-V2, pp 39-1−39-13.

(13) Hower, J. C.; Rathbone, R. F.; Robl, T. L.; Thomas, G. A.; Haeberlin, B. O.; Trimble, A. S. Case study of the conversion of tangential- and wall-fired units to low-NO_x combustion: Impact on fly ash quality. *Waste Manage.* **1998**, *17*, 219−229.

(14) Hower, J. C.; Graham, U. M.; Wong, A. S.; Robertson, J. D.; Haeberlin, B. O.; Thomas, G. A.; Schram, W.H. Influence of flue-gas desulfurization on coal combustion by-product quality at Kentucky power stations burning high-sulfur coal. *Waste Manage.* **1998**, *17*, 523−533.

(15) Hower, J. C.; Robl, T. L.; Thomas, G.A. Changes in the Quality of Coal Combustion By-products Produced by Kentucky Power Plants, 1978 to 1997: Consequences of Clean Air Act Directives. *Fuel* **1999**, *78*, 701−712.

(16) Hower, J. C.; Robl, T. L.; Thomas, G. A. Changes in the quality of coal delivered to Kentucky power plants, 1978 to 1997: Responses to Clean Air Act directives. *Int. J. Coal Geol.* **1999**, *41*, 125−155.

(17) Hower, J. C.; Thomas, G. A.; Palmer, J. Impact of the conversion to low-NO_x combustion on ash characteristics in a utility boiler burning Western US coal. *Fuel Process. Technol.* **1999**, *61*, 175−195.

(18) Hower, J. C.; Robl, T. L.; Anderson, C.; Thomas, G. A.; Sakulpitakphon, T.; Mardon, S. M.; Clark, W. L. Characteristics of coal utilization products (CUBs) from Kentucky power plants, with emphasis on Mercury content. *Fuel* **2005**, *84*, 1338−1350.

(19) Hower, J. C.; Sakulpitakphon, T.; Trimble, A. S.; Thomas, G. A.; Schram, W. H. Asymmetry of major and minor element distribution in fly ash from a coal-fired utility boiler in Kentucky. *Energy Sources, Part A* **2006**, *28*, 79−95.

(20) Hower, J. C.; Robertson, J. D.; Elswick, E. R.; Roberts, J. M.; Brandsteder, K.; Trimble, A. S.; Mardon, S. M. Further investigation of the impact of the co-combustion of tire-derived fuel and petroleum coke on the petrology and chemistry of coal combustion products. *Energy Sources, Part A* **2007**, *29*, 439−461.

(21) Hower, J. C.; Robl, T. L.; Thomas, G. A.; Hopps, S. D.; Grider, M. Chemistry of coal and coal combustion products from Kentucky power plants: Results from the 2007 sampling, with emphasis on selenium. *Coal Combust. Gasif. Prod.* **2009**, *1*, 50−62, http://www.coalcgp-journal.org/papers/2009/CCGP-D-09-00013-Hower-supp.pdf,.

(22) Sakulpitakphon, T.; Hower, J. C.; Trimble, A. S.; Schram, W. H.; Thomas, G. A. Mercury capture by fly ash: Study of the combustion of a high-mercury coal at a utility boiler. *Energy Fuels* **2000**, *14*, 727−733.

(23) Sakulpitakphon, T.; Hower, J. C.; Trimble, A. S.; Thomas, G. A.; Schram, W. H. Arsenic and Mercury Partitioning in Fly Ash at a Kentucky Power Plant. *Energy Fuels* **2003**, *17*, 1028−1033.

(24) Sakulpitakphon, T.; Hower, J. C.; Schram, W. H.; Ward, C. R. Tracking Mercury from the Mine to the Power Plant: Geochemistry of the Manchester Coal Bed, Clay County, Kentucky. *Int. J. Coal Geol.* **2004**, *57*, 127−141.

(25) Pires, M.; Querol, X. Characterization of Candiota (South Brazil) coal and combustion by-product. *Int. J. Coal Geol.* **2004**, *60*, 57−72.

(26) Mardon, S. M.; Hower, J. C. Impact of coal properties on coal combustion by-product quality: Examples from a Kentucky power plant. *Int. J. Coal Geol.* **2004**, *59*, 153−169.

DOI: 10.1021/acs.energyfuels.5b02033
Energy Fuels 2015, 29, 7168−7177

(27) Mastalerz, M.; Hower, J. C.; Drobniak, A.; Mardon, S. M.; Lis, G. From in-situ coal to fly ash: A study of coal mines and power plants from Indiana. *Int. J. Coal Geol.* **2004**, *59*, 171−192.
(28) Suárez-Ruiz, I.; Hower, J. C.; Thomas, G. A. Hg and Se capture and fly ash carbons from combustion of complex pulverized feed blends mainly of anthracitic coal rank in Spanish power plants. *Energy Fuels* **2007**, *21*, 59−70.
(29) Hochella, M. F.; Lower, S. K.; Maurice, P. A.; Penn, R. L.; Sahai, N.; Sparks, D. L.; Twining, B. S. Nanominerals, mineral nanoparticles, and Earth systems. *Science* **2008**, *319*, 1631−1635.
(30) Wigginton, N. S.; Haus, K. L.; Hochella, M. F., Jr. Aquatic environmental nanoparticles. *J. Environ. Monit.* **2007**, *9*, 1306−1316.
(31) Ribeiro, J.; DaBoit, K.; Flores, D.; Kronbauer, M. A.; Silva, L. F. O. Extensive FE-SEM/EDS, HR-TEM/EDS and ToF-SIMS studies of micron- to nano-particles in anthracite fly ash. *Sci. Total Environ.* **2013**, *452*−*453*, 98−107.
(32) Ribeiro, J.; Taffarel, S. R.; Sampaio, C. H.; Flores, D.; Silva, L. F. O. Mineral speciation and fate of some hazardous contaminants in coal waste pile from anthracite mining in Portugal. *Int. J. Coal Geol.* **2013**, *109*−*110*, 15−23.
(33) Silva, L. F. O.; DaBoit, K.; Sampaio, C. H.; Jasper, A.; Andrade, M. L.; Kostova, I. J.; Waanders, F. B.; Henke, K. R.; Hower, J. C. The occurrence of hazardous volatile elements and nanoparticles in Bulgarian coal fly ashes and the effect on human health exposure. *Sci. Total Environ.* **2012**, *416*, 513−526.
(34) Silva, L. F. O.; Sampaio, C. H.; Guedes, A.; Fdez-Ortiz de Vallejuelo, S.; Madariaga, J. M. Multianalytical approaches to the characterisation of minerals associated with coals and the diagnosis of their potential risk by using combined instrumental microspectroscopic techniques and thermodynamic speciation. *Fuel* **2012**, *94*, 52−63.
(35) Hower, J. C.; Robertson, J. D.; Thomas, G. A.; Wong, A. S.; Schram, W. H.; Graham, U. M.; Rathbone, R. F.; Robl, T. L. Characterization of fly ash from Kentucky power plants. *Fuel* **1996**, *75*, 403−411.
(36) Hower, J. C.; Thomas, G. A.; Hopps, S. G. Trends in coal utilization and coal-combustion product production in Kentucky: Results of the 2012 survey of power plants. *Coal Combust. Gasif. Prod.* **2014**, *6*, 35−41.
(37) Hower, J. C.; Bland, A. E. Geochemistry of the Pond Creek Coal Bed, Eastern Kentucky Coalfield. *Int. J. Coal Geol.* **1989**, *11*, 205−226.
(38) Hower, J. C. Petrographic examination of coal-combustion fly ash. *Int. J. Coal Geol.* **2012**, *92*, 90−97.
(39) Giannuzzi, L. A.; Prenitzer, B. I.; Drown-Macdonald, J. L.; Shofner, T. L.; Brown, S. R.; Irwin, R. B.; Stevie, F. A. Electron microscopy sample preparation for the biological and physical sciences using focused ion beams. *J. Process Anal. Chem.* **1999**, *4*, 162−167.
(40) International Centre for Diffraction Data (ICDD). *The Powder Diffraction File*; ICDD: Newtown Square, PA, 2015; http://www.icdd.com/.
(41) Dai, S.; Zhao, L.; Hower, J. C.; Johnston, M. N.; Song, W.; Wang, P.; Zhang, S. Petrology, mineralogy, and chemistry of size-fractioned fly ash from the Jungar power plant, Inner Mongolia, China, with emphasis on the distribution of rare earth elements. *Energy Fuels* **2014**, *28*, 1502−1514.
(42) Hower, J. C.; Dai, S.; Seredin, V. V.; Zhao, L.; Kostova, I. J.; Silva, L. F. O.; Mardon, S. M.; Gurdal, G. A note on the occurrence of Yttrium and Rare Earth Elements in coal combustion products. *Coal Combust. Gasif. Prod.* **2013**, *5*, 39−47.
(43) Hower, J. C.; Graham, U. M.; Dozier, A.; Tseng, M. T.; Khatri, R. A. Association of sites of heavy metals with nanoscale carbon in a Kentucky electrostatic precipitator fly ash. *Environ. Sci. Technol.* **2008**, *42*, 8471−8477.
(44) Silva, L. F. O.; DaBoit, K.; Serra, C.; Mardon, S. M.; Hower, J. C. Fullerenes and metallofullerenes in coal-fired stoker fly ash. *Coal Combust. Gasif. Prod.* **2010**, *2*, 66−79.
(45) Mardon, S. M.; Hower, J. C.; O'Keefe, J. M. K.; Marks, M. N.; Hedges, D. H. Coal combustion by-product quality at two stoker boilers: Coal source versus fly ash collection system design. *Int. J. Coal Geol.* **2008**, *75*, 248−254.

DOI: 10.1021/acs.energyfuels.5b02033
Energy Fuels 2015, 29, 7168−7177